CSMA 2019
14ème Colloque National en Calcul des Structures
13-17 Mai 2019, Presqu'île de Giens (Var)

On the non-quadratic defect energy in strain gradient crystal plasticity

Lei CAI[1], Mohamed JEBAHI[1], Farid ABED-MERAIM[1]

[1] *Arts et Métiers ParisTech, CNRS, Université de Lorraine, LEM3, 57000 Metz, France*
{lei.cai, Mohamed.Jebahi, Farid.Abed-Meraim}@ensam.eu

Résumé — Strain gradient crystal plasticity (SGCP) represents a very promising way to account for size effects in miniaturized components, thanks to the intrinsic length scale(s) embedded. Most of the existing SGCP models are based on a quadratic form of defect energy. However, it has recently been shown that this form leads to physically unrealistic results concerning the size-dependence of the mechanical response of miniaturized components. A generalized non-quadratic form is proposed in this work which aims to study the influence of the defect energy order on the global response of size-dependent materials.
Mots clés — Strain gradient crystal plasticity, size effects, generalized defect energy, non-quadratic form

1 Introduction

In recent years, there has been a great demand for miniaturized products in many high-technology fields such as microelectronics, microbotics and micromedicine due to the advantages in terms of higher material utilizing rate, higher productivity and better mechanical performance. However, when the dimensions of miniaturized products are in the range of few tens of micrometers, the flow strength is no longer scale-independent and the peculiar phenomenon "smaller is stronger" appears. Conventional plasticity theories cannot predict the size-dependent behavior, due to the lack of intrinsic length scale(s) allowing for correct prediction of gradient effects. To overcome this limitation, Aifantis [1] has proposed in a pioneering work a strain gradient plasticity (SGP) model. The attractive idea of such a model has led to the development of a wide variety of SGP models for single- and poly-crystal structures in the last two decades.

Most applications involving strain gradient crystal plasticity (SGCP) theories are based on quadratic formulations of defect energy which function as a linkage between free energy and dislocation densities and gradients of plastic slips [2, 3, 4, 5, 6, 7]. As an example, the defect energy in the formulation of Gurtin *et al*. [3] was defined as a quadratic form of dislocation densities. However, investigation conducted by Fleck and Willis [8] shows that this choice is not always in accordance with the physics behind dislocation mechanisms. Some preliminary results by Evans and Hutchinson [9] suggested that defect energy should be nearly linear. Cordero *et al*. [10] and Forest and Gueninchault [11] recently showed that the quadratic form leads to physically unrealistic scaling in the size-dependent response of laminated microstructures under shear, since quadratic forms are not usual in classical dislocation theory. Rank-one defect energy, which is linear with respect to dislocation densities, has been used by several authors [12, 13, 14]. This form of defect energy leads to an increased macroscopic yield stress in certain situations. Logarithmic defect energy as function of dislocation density tensor has also been proposed by Forest *et al*. [5, 11]. Despite the research effort on the subject, elaboration of an optimal form of defect energy remains very challenging. Using a generalized power-law defect energy, the present work tries to investigate the influence of the defect energy index on the global response of materials.

After this introduction, the paper is organized as follows. Section 2 details the developed strain gradient crystal plasticity model based on a generalized non-quadratic (power-law) form of defect energy. Section 3 investigates the influence of the order of the proposed defect energy on the global response of a constrained two-dimensional crystalline strip subjected to shear loading. Section 4 provides some concluding remarks.

2 Formulation of strain gradient crystal plasticity model

2.1 Kinematics

Let $\mathbf{u}(\mathbf{x},t)$ denotes the displacement at time t of an arbitrary material point identified by $\mathbf{x}$ in a subregion $\mathcal{V}$ of the considered continuum. In the framework of small deformation, the displacement gradient $\boldsymbol{\nabla}\mathbf{u}$ can be additively split into elastic and plastic parts :

$$\boldsymbol{\nabla}\mathbf{u} = \mathbf{H}_e + \mathbf{H}_p \tag{1}$$

$\mathbf{H}_e$ represents the elastic distortion associated with stretch and rotation of the underlying lattice, $\mathbf{H}_p$ represents the plastic distortion due to plastic flow.

In single-crystal plasticity framework, it is widely acknowledged that plastic flow occurs through slip on prescribed slip systems, with each system α defined by a slip direction vector $\mathbf{s}^\alpha$ and a slip-plane normal vector $\mathbf{m}^\alpha$. These vectors will be assumed to remain constant during the deformation process and to verify :

$$\|\mathbf{s}^\alpha\| = \|\mathbf{m}^\alpha\| = 1 \quad \text{and} \quad \mathbf{s}^\alpha \perp \mathbf{m}^\alpha \tag{2}$$

With this description of plastic flow, the rate of $\mathbf{H}_p$ can be expressed as follows :

$$\dot{\mathbf{H}}_p = \sum_{\alpha=1}^{ns} \dot{\gamma}^\alpha \left[\mathbf{s}^\alpha \otimes \mathbf{m}^\alpha\right] \tag{3}$$

where $\dot{\gamma}^\alpha$ is the rate of plastic slip on slip system α, *ns* is the total number of slip systems, and "$\otimes$" is the tensor product operator. In what follows, $\boldsymbol{\gamma}$ and $\dot{\boldsymbol{\gamma}}$ (in bold) will be used to designate the list of plastic slips and their rates, respectively :

$$\boldsymbol{\gamma} = \left(\gamma^1, \gamma^2, \cdots, \gamma^{ns}\right), \; \dot{\boldsymbol{\gamma}} = \left(\dot{\gamma}^1, \dot{\gamma}^2, \cdots, \dot{\gamma}^{ns}\right) \tag{4}$$

Using (3), the plastic strain rate tensor $\dot{\boldsymbol{\varepsilon}}_p$ can be obtained as function of $\dot{\boldsymbol{\gamma}}$ as follows :

$$\dot{\boldsymbol{\varepsilon}}_p = \sum_{\alpha=1}^{ns} \dot{\gamma}^\alpha \mathbf{P}^\alpha \tag{5}$$

where $\mathbf{P}^\alpha$ is the symmetrized Schmid tensor associated with slip system α :

$$\mathbf{P}^\alpha = \frac{1}{2}\left(\mathbf{s}^\alpha \otimes \mathbf{m}^\alpha + \mathbf{m}^\alpha \otimes \mathbf{s}^\alpha\right) \tag{6}$$

2.2 Balance equations

In the considered enhanced continuum, both displacement and plastic slip fields are considered as primary and controllable variables. With this in mind, the balance equations of the proposed SGCP model will be derived, hereafter, using the principle of virtual power. The internal virtual power expended within a subregion $\mathcal{V}$ of the considered continuum can be expressed as follows :

$$\mathcal{P}_{int} = \int_{\mathcal{V}} \boldsymbol{\sigma} : \delta\dot{\boldsymbol{\varepsilon}}_e \, dv + \sum_{\alpha=1}^{ns} \int_{\mathcal{V}} \pi^\alpha \delta\dot{\gamma}^\alpha \, dv + \sum_{\alpha=1}^{ns} \int_{\mathcal{V}} \boldsymbol{\xi}^\alpha \cdot \delta\boldsymbol{\nabla}\dot{\gamma}^\alpha \, dv \tag{7}$$

where $\boldsymbol{\sigma}$ is macroscopic stress tensor, π^α and $\boldsymbol{\xi}^\alpha$ are respectively microscopic stress scalar and microscopic stress vector associated with slip system α. Assuming that no external body forces act on the subregion $\mathcal{V}$ and the contact forces acting on its boundary $\mathcal{S}$ can be represented by a macroscopic traction vector $\mathbf{t}$ and a microscopic traction scalar χ^α on each slip system α, the external virtual power expended on $\mathcal{V}$ can be expressed as :

$$\mathcal{P}_{ext} = \int_{\mathcal{S}} \mathbf{t} \cdot \delta\dot{\mathbf{u}} \, ds + \sum_{\alpha=1}^{ns} \int_{\mathcal{S}} \chi^\alpha \delta\dot{\gamma}^\alpha \, ds \tag{8}$$

Application of the virtual power principle, which postulates that the internal and external virtual powers are balanced for any subregion $\mathcal{V}$ and virtual variations of the modeling variables, leads to two kinds of

balance equations (since two kinds of primary variables are used). Macroscopic balance equations can be obtained by setting :

$$\delta\dot{\boldsymbol{\gamma}} = \mathbf{0} \quad (\text{i.e., } \delta\boldsymbol{\nabla}\dot{\mathbf{u}} = \delta\dot{\boldsymbol{\varepsilon}}_e + \delta\dot{\boldsymbol{\omega}}_e) \tag{9}$$

Considering the symmetry of the stress tensor $\boldsymbol{\sigma}$, the virtual power balance becomes :

$$\int_{\mathcal{V}} \boldsymbol{\sigma} : \delta\boldsymbol{\nabla}\dot{\mathbf{u}}\, dv = \int_{\mathcal{S}} \mathbf{t} \cdot \delta\dot{\mathbf{u}}\, ds \tag{10}$$

or, after application of the Gauss (divergence) theorem :

$$\int_{\mathcal{V}} (\boldsymbol{\nabla} \cdot \boldsymbol{\sigma}) \cdot \delta\dot{\mathbf{u}}\, dv = \int_{\mathcal{S}} (\boldsymbol{\sigma} \cdot \mathbf{n} - \mathbf{t}) \cdot \delta\dot{\mathbf{u}}\, ds \tag{11}$$

which is valid for any arbitrary subregion $\mathcal{V}$ and virtual variations of the modeling variables. This leads to the classical balance equations (static case) and the well-known traction conditions :

$$\left\{ \begin{array}{rcll} \boldsymbol{\nabla} \cdot \boldsymbol{\sigma} & = & \mathbf{0} & \text{in } \mathcal{V} \\ \boldsymbol{\sigma} \cdot \mathbf{n} & = & \mathbf{t} & \text{on } \mathcal{S} \end{array} \right. \tag{12}$$

with $\mathbf{n}$ the outward unit normal to $\mathcal{S}$. The microscopic counterparts of these balance equations and boundary conditions can be obtained by setting :

$$\delta\dot{\mathbf{u}} = \mathbf{0} \quad (i.e.,\ \delta\dot{\boldsymbol{\varepsilon}}_e + \delta\dot{\boldsymbol{\omega}}_e = -\sum_{\alpha=1}^{ns} \delta\dot{\gamma}^\alpha \mathbf{s}^\alpha \otimes \mathbf{m}^\alpha) \tag{13}$$

Considering (13), it can be demonstrated that :

$$\boldsymbol{\sigma} : \delta\dot{\boldsymbol{\varepsilon}}_e = -\sum_{\alpha=1}^{ns} \tau^\alpha\, \delta\dot{\gamma}^\alpha \tag{14}$$

where τ^α is the resolved shear stress on slip system α defined by $\tau^\alpha = \boldsymbol{\sigma} : \mathbf{P}^\alpha$. This leads, after application of the Gauss theorem, to the following form of the virtual power balance :

$$\sum_{\alpha=1}^{ns} \int_{\mathcal{V}} (\tau^\alpha + \boldsymbol{\nabla} \cdot \boldsymbol{\xi}^\alpha - \pi^\alpha)\, \delta\dot{\gamma}^\alpha\, dv = \sum_{\alpha=1}^{ns} \int_{\mathcal{S}} (\boldsymbol{\xi}^\alpha \cdot \mathbf{n} - \chi^\alpha)\, \delta\dot{\gamma}^\alpha\, ds = 0 \tag{15}$$

Since (15) is valid for any arbitrary subregion $\mathcal{V}$ and virtual variations of the modeling variables, the microscopic balance equation (static case) and the microscopic traction condition on each slip system α can be obtained :

$$\left\{ \begin{array}{rcll} \tau^\alpha + \boldsymbol{\nabla} \cdot \boldsymbol{\xi}^\alpha - \pi^\alpha & = & 0 & \text{in } \mathcal{V} \\ \boldsymbol{\xi}^\alpha \cdot \mathbf{n} & = & \chi^\alpha & \text{on } \mathcal{S} \end{array} \right. \tag{16}$$

2.3 Constitutive laws based on non-quadratic defect energy

In this work, $\boldsymbol{\sigma}$ and $\boldsymbol{\xi}^\alpha$ ($\alpha \in \{1, 2, ..., ns\}$) are regarded as energetic and to be derived from the free energy density ψ, which is assumed to be decomposed into an elastic part ψ_e and a defect energy part ψ_p. The elastic part ψ_e is assumed to be a quadratic in $\boldsymbol{\varepsilon}_e$:

$$\psi_e(\boldsymbol{\varepsilon}_e) = \frac{1}{2}\, \boldsymbol{\varepsilon}_e : \mathbf{C} : \boldsymbol{\varepsilon}_e \tag{17}$$

where $\mathbf{C}$ is the elasticity tensor, which is assumed to be symmetric and positive-definite. Building on the work of Gurtin *et al.* [3], ψ_p is assumed to be function of dislocation densities :

$$\boldsymbol{\rho} = \left(\rho_{\vdash}^1, \rho_{\vdash}^2, ..., \rho_{\vdash}^{ns}, \rho_{\odot}^1, \rho_{\odot}^2, ..., \rho_{\odot}^{ns}\right) \tag{18}$$

where $\rho_{\vdash}^\alpha$ and $\rho_{\odot}^\alpha$ denote respectively edge and screw dislocation densities on slip system α. As shown by Arsenlis and Parks [15], these quantities can be calculated by :

$$\rho_{\vdash}^\alpha = -\mathbf{s}^\alpha \cdot \boldsymbol{\nabla}\gamma^\alpha,\ \rho_{\odot}^\alpha = \mathbf{l}^\alpha \cdot \boldsymbol{\nabla}\gamma^\alpha \tag{19}$$

where $\mathbf{l}^\alpha$ is the line direction of dislocation distribution defined by $\mathbf{l}^\alpha = \mathbf{m}^\alpha \times \mathbf{s}^\alpha$ ("$\times$" is cross product operator). In the literature, ψ_p is generally considered to be a quadratic function of the plastic strain gradients or equivalent [2, 3, 4, 16]. However, Fleck *et al.* [17] have shown in a recent work that this choice can lead to incorrect results concerning the contribution of recoverable gradient effects to the behavior of materials. Using a non-quadratic defect energy of order $n = 1.2$ and monotonic loadings, these authors have demonstrated that such effects contribute not only to hardening as widely recognized but also to strengthening. To enrich the discussions about this point, a generalized n-order form of ψ_p will be used in the present paper :

$$\psi_p(\boldsymbol{\nabla\gamma}) = \frac{1}{n} X_0 \, l_{en}^n \sum_{\alpha=1}^{ns} \left[|\rho_{\vdash}^\alpha|^n + |\rho_{\odot}^\alpha|^n \right] \tag{20}$$

where n is defect energy index, X_0 is a constant representing the energetic slip resistance, l_{en} is an energetic length scale. To ensure the convexity of ψ_p, the defect energy index must be greater than 1 ($n > 1$). Using (17) and (20), the free energy density can be expressed as :

$$\psi(\boldsymbol{\varepsilon}_e, \boldsymbol{\nabla\gamma}) = \frac{1}{2} \boldsymbol{\varepsilon}_e : \mathbf{C} : \boldsymbol{\varepsilon}_e + \frac{1}{n} X_0 \, l_{en}^n \sum_{\alpha=1}^{ns} \left[|\rho_{\vdash}^\alpha|^n + |\rho_{\odot}^\alpha|^n \right] \tag{21}$$

The partial derivatives of this expression with respect to the state variables provide the energetic constitutive laws that describe the evolution of $\boldsymbol{\sigma}$ and $\boldsymbol{\xi}^\alpha$ ($\alpha \in \{1, 2, ..., ns\}$). The macroscopic (energetic) stress tensor $\boldsymbol{\sigma}$ can be expressed as :

$$\boldsymbol{\sigma} = \frac{\partial \psi}{\partial \boldsymbol{\varepsilon}_e} = \mathbf{C} : \boldsymbol{\varepsilon}_e \tag{22}$$

or, in the rate form (since $\mathbf{C}$ is constant), as :

$$\dot{\boldsymbol{\sigma}} = \mathbf{C} : \dot{\boldsymbol{\varepsilon}}_e \tag{23}$$

The microscopic energetic stress vector $\boldsymbol{\xi}^\alpha$ can be expressed as :

$$\boldsymbol{\xi}^\alpha = \frac{\partial \psi_p}{\partial \nabla\gamma^\alpha} \tag{24}$$

After calculation, $\boldsymbol{\xi}^\alpha$ can be rewritten as :

$$\boldsymbol{\xi}^\alpha = X_0 \, l_{en}^n \left\{ |\boldsymbol{s}^\alpha \cdot \boldsymbol{\nabla\gamma}^\alpha|^{n-2} \, \boldsymbol{s}^\alpha \otimes \boldsymbol{s}^\alpha + |\boldsymbol{l}^\alpha \cdot \boldsymbol{\nabla\gamma}^\alpha|^{n-2} \, \boldsymbol{l}^\alpha \otimes \boldsymbol{l}^\alpha \right\} \cdot \boldsymbol{\nabla\gamma}^\alpha \tag{25}$$

Concerning the microscopic stress scalars π^α ($\alpha \in \{1, 2, ..., ns\}$), they are assumed, in this work, to be fully dissipative and to be simply expressed as :

$$\pi^\alpha = Y_0 \left| \frac{\dot{\gamma}^\alpha}{\dot{\gamma}_0^\alpha} \right|^m \text{sign}(\dot{\gamma}^\alpha) \tag{26}$$

where Y_0 is a strictly positive constant representative of slip resistance, $\dot{\gamma}_0^\alpha > 0$ is a constant strain rate representative of the flow rates of interest, and $m > 0$ is a constant characterizing the rate sensitivity of the considered material.

3 Influence of the defect energy index n

In order to investigate the influence of the defect energy index n on the global response of the considered continuum, a simplified two-dimensional (2D) version of the proposed SGCP model, under plane strain condition, is implemented within the commercial finite element package Abaqus/Standard, with the help of User-ELment (UEL) subroutine. This implemented version is then applied to simulate a simple shear problem of a constrained 2D strip of height h and width w [18]. Two slip systems, symmetrically oriented with respect to x_1 axis ($\theta_1 = -\theta_2 = 60^\circ$), are taken into account in this strip. The bottom edge is totally fixed and the top edge is subject to linear displacement loading along x_1 direction. Micro-clamped

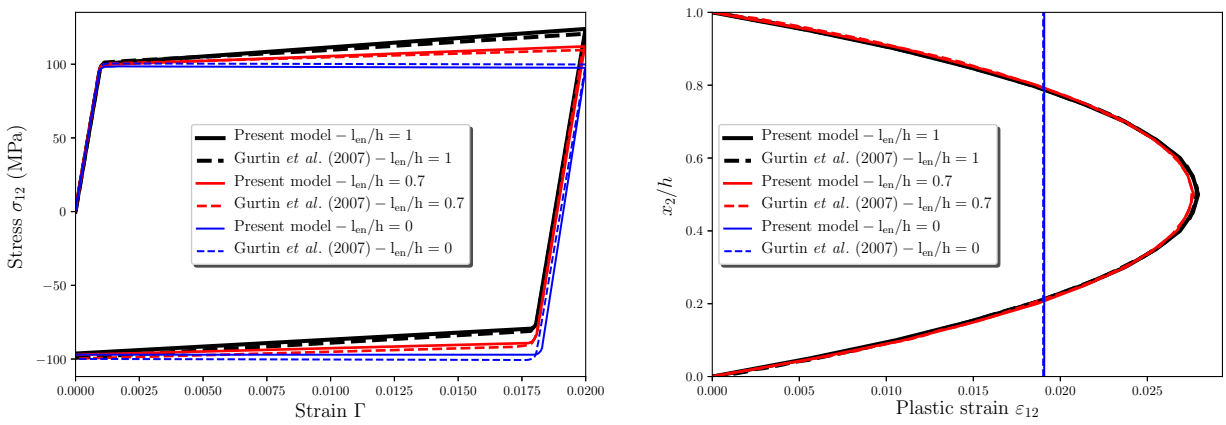

(a) Stress-strain curves

(b) plastic shear strain distributions along $\mathbf{e}_2$ direction

FIGURE 1 – Influence of the energetic length scale l_{en} in the case of quadratic defect energy ($X_0 = Y_0 = 50\,\text{MPa}$, $n = 2$)

boundary conditions are also applied on the top and bottom edges ($\gamma^1 = \gamma^2 = 0$ on these edges). Finally, periodical conditions (with period w) are imposed on the left and right edges to model the infinite length of the strip.

Starting with $n = 2$ (quadratic defect energy), fig. 1 presents the influence of the energetic length scale on the global response of the considered strip. Results of this figure, which are obtained using $X_0 = Y_0 = 50\,\text{MPa}$, are in very good agreement with those obtained by Gurtin *et al.* [3] using similar consititutive parameters. As expected, for quadratic defect energy, the energetic length scale contributes to hardening but not to strengthening. In all stress-strain curves (fig. 1a), plasticity starts from the same yield point and different hardening rates take place after yielding when varying l_{en}/h. The case of $l_{en}/h = 0$ gives a flat stress-strain curve with no hardening after yielding and the plastic shear strain distribution though the strip thickness is uniform. It corresponds to the classical crystal plasticity (CP) with no hardening (simply designated by "Perfect CP" in subsequent figures). For $l_{en}/h = 0.7$ and $l_{en}/h = 1$, kinematic hardening occurs, leading to Bauschinger effects which become more marked with increasing l_{en}/h. The associated plastic shear strain distributions present a quadratic form (Fig. 1b).

Considering the case of non-quadratic defect energy with $n < 2$, Fig. 2 presents the stress-strain curves and the plastic shear strain profiles for different values of n (with $n < 2$) and different values of l_{en}/h. As is shown in Fig. 2a, by analyzing only loading part of the results, the energetic length scale seems to contribute to material strengthening as reported by Fleck *et al.* [8] in their study based only on monotonic loadings. The smaller the value of n (*i.e.*, n approaches 1), the larger is the contribution of l_{en} to this phenomenon. However, by analyzing the entire loading-unloading results, a striking feature that can be noted is the presence of inflection points in the stress-strain curves. Actually, the material only experienced an unusual pure nonlinear kinematic hardening (Fig. 2a). In the framework of SGCP, this type of kinematic hardening was first reported by Ohno *et al.* [19], using rank-one defect energy. However, the authors did not recognize the physical origin of this phenomenon. Instead, they further developed their model to replace the rank-one defect energy by a dissipative formulation removing the inflection points. In interesting recent works, Forest *et al.* [5, 20] have also obtained such a phenomenon using rank-one and logarithmic defect energies. These authors were the first to provide a physical explanation of the phenomenon in the context of SGCP. Based on their works [5, 20], the obtained nonlinear kinematic hardening corresponds to the kinematic hardening type III (KIII) of Asaro [21]. This type corresponds to a "first in/last out" sequence of dislocation motion and represents the most perfect form of recovery of plastic memory. It was already observed experimentally in several materials, such as some polycrystalline Fe-Cr and Al-Cu-Mg alloys. Using a defect energy of order $n < 2$, KIII type hardening is the single active hardening mechanism, allowing for accurate continuum description of the piling-up and unpiling-up phenomena. This hardening type results in flattening the parabolic plastic shear strain distribution observed with $n = 2$ and leads to the formation of a central region with uniform plastic shear

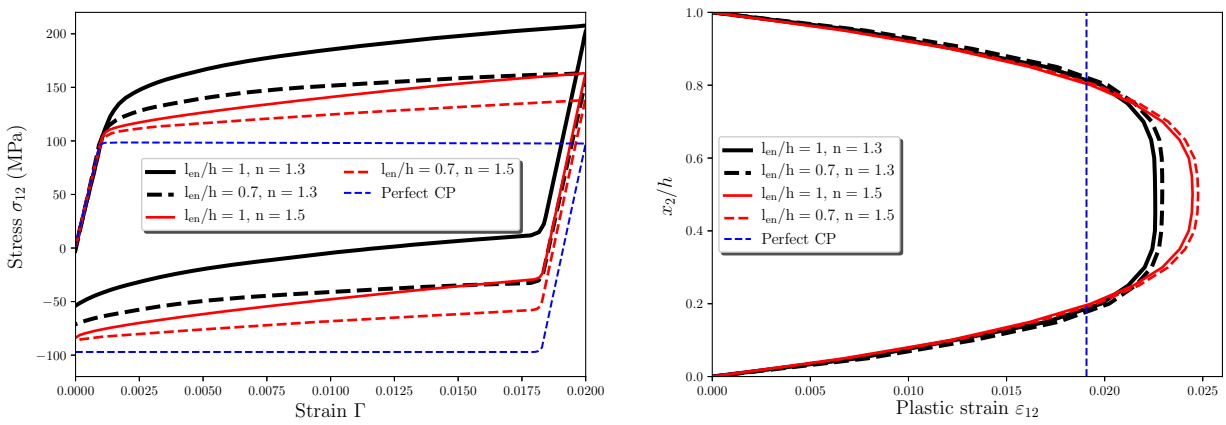

(a) Stress-strain curves

(b) Plastic shear strain distributions along $\mathbf{e}_2$ direction

FIGURE 2 – Interaction between the energetic length scale l_{en} and the defect energy index n in the range of $n < 2$ ($X_0 = Y_0 = 50\,\text{MPa}$)

strain (Fig. 2b).

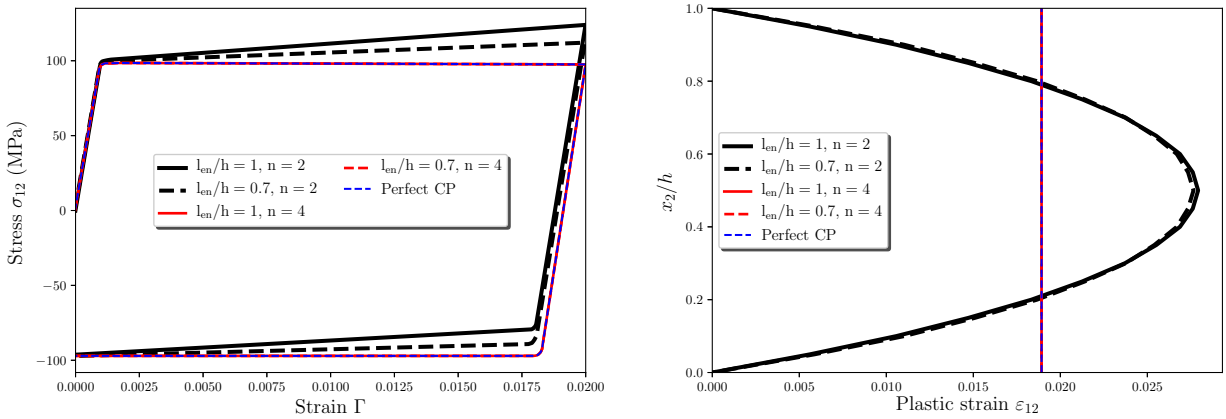

(a) Stress-strain curves

(b) Plastic-shear strain distributions along $\mathbf{e}_2$ direction

FIGURE 3 – Interaction between the energetic length scale l_{en} and the defect energy index n in the range of $n \geq 2$ ($X_0 = Y_0 = 50\,\text{MPa}$)

Studying the case of non-quadratic defect energy with $n \geq 2$, Fig. 3 shows the stress-strain results and the associated plastic shear strain profiles for $n \geq 2$. From $n = 2$, the KIII type hardening disappears and is replaced by the classical kinematic hardening (KI type hardening, in the terminology of Asaro [21]). In this case, l_{en} has no longer contribution to the strengthening-like phenomenon observed using $n < 2$. As illustrated in Fig. 3a , in the range of $n \geq 2$, l_{en} has only effects on the rate of classical hardening which decrease with increasing n. A large value of n can even cancel these effects of l_{en} (case of $n = 4$ in Fig. 3a). Using large n, the microscopic stress vectors $\boldsymbol{\xi}^{\alpha}$ become insensitive to small variations in the gradient of the plastic slips. In this case, the material behaves as if $\boldsymbol{\xi}^{\alpha} = 0$ (*i.e.*, $l_{en} = 0$) and the plastic shear strains become uniformly distributed across the strip thickness (Fig. 3b).

4 Conclusions

In this work, a general non-quadratic power-law form of defect energy with an order-controlling index n has been proposed to investigate the influence of this parameter on material response. Based on the results of this work, the following conclusions can be drawn. In the range of $n < 2$, the energetic length

scale leads to an unusual nonlinear kinematic hardening which complies with the kinematic hardening type III (KIII) of Asaro [22]. This type corresponds to a "first in/last out" sequence of dislocation motion and represents the most perfect form of recovery of plastic memory. It is the single active hardening mechanism, allowing for accurate continuum description of the piling-up and unpiling-up phenomena. Beyond $n = 2$, the nonlinear hardening (KIII type hardening) vanishes and classical kinematic hardening recovers . In this case, l_{en} only influences the hardening rate but not the value of the initial yield strength (as it is the case for $n < 2$). The hardening effects of l_{en} are inversely related to the value of $n > 2$.

Références

[1] E. C. Aifantis. On the Microstructural Origin of Certain Inelastic Models. *Journal of Engineering Materials and Technology*, 106(4) :326, oct 1984.

[2] M. E. Gurtin. A gradient theory of single-crystal viscoplasticity that accounts for geometrically necessary dislocations. *Journal of the Mechanics and Physics of Solids*, 50(1) :5–32, 2002.

[3] M. E. Gurtin, L. Anand, and S. P. Lele. Gradient single-crystal plasticity with free energy dependent on dislocation densities. *Journal of the Mechanics and Physics of Solids*, 55(9) :1853–1878, sep 2007.

[4] B. D. Reddy. The role of dissipation and defect energy in variational formulations of problems in strain-gradient plasticity. Part 1 : polycrystalline plasticity. *Continuum Mechanics and Thermodynamics*, 23(6) :527–549, nov 2011.

[5] S. Wulfinghoff, S. Forest, and T. Böhlke. Strain gradient plasticity modeling of the cyclic behavior of laminate microstructures. *Journal of the Mechanics and Physics of Solids*, 79 :1–20, 2015.

[6] B.D. Reddy, C. Wieners, and B. Wohlmuth. Finite element analysis and algorithms for single-crystal strain-gradient plasticity. *International Journal for Numerical Methods in Engineering*, 90(6) :784–804, may 2012.

[7] L. Bardella. A deformation theory of strain gradient crystal plasticity that accounts for geometrically necessary dislocations. *Journal of the Mechanics and Physics of Solids*, 54(1) :128–160, jan 2006.

[8] N. A. Fleck and J. R. Willis. Strain gradient plasticity : energetic or dissipative ? *Acta Mechanica Sinica*, 31(4) :465–472, aug 2015.

[9] A. G. Evans and J. W. Hutchinson. A critical assessment of theories of strain gradient plasticity. *Acta Materialia*, 57(5) :1675–1688, mar 2009.

[10] A. Gaubert, S. Kruch, N.M. Cordero, F. Gallerneau, E.P. Busso, and S. Forest. Size effects in generalised continuum crystal plasticity for two-phase laminates. *Journal of the Mechanics and Physics of Solids*, 58(11) :1963–1994, nov 2010.

[11] S. Forest and N. Guéninchault. Inspection of free energy functions in gradient crystal plasticity. *Acta Mechanica Sinica/Lixue Xuebao*, 29(6) :763–772, 2013.

[12] N. Ohno and D. Okumura. Higher-order stress and grain size effects due to self-energy of geometrically necessary dislocations. *Journal of the Mechanics and Physics of Solids*, 55(9) :1879–1898, sep 2007.

[13] D. E. Hurtado and M. Ortiz. Finite element analysis of geometrically necessary dislocations in crystal plasticity. *International Journal for Numerical Methods in Engineering*, 93(1) :66–79, jan 2013.

[14] R. Kametani, K. Kodera, D. Okumura, and N. Ohno. Implicit iterative finite element scheme for a strain gradient crystal plasticity model based on self-energy of geometrically necessary dislocations. *Computational Materials Science*, 53(1) :53–59, feb 2012.

[15] A. Arsenlis and D. M. Parks. Crystallographic aspects of geometrically-necessary and statistically-stored dislocation density. *Acta Materialia*, 47(5) :1597–1611, mar 1999.

[16] B. D. Reddy. The role of dissipation and defect energy in variational formulations of problems in strain-gradient plasticity. Part 2 : single-crystal plasticity. *Continuum Mechanics and Thermodynamics*, 23(6) :551–572, nov 2011.

[17] N. A. Fleck, J. W. Hutchinson, and J. R. Willis. Guidelines for Constructing Strain Gradient Plasticity Theories. *Journal of Applied Mechanics*, 82(7) :071002, jul 2015.

[18] E. Bittencourt, A. Needleman, M.E. Gurtin, and E. Van der Giessen. A comparison of nonlocal continuum and discrete dislocation plasticity predictions. *Journal of the Mechanics and Physics of Solids*, 51(2) :281–310, feb 2003.

[19] N. Ohno, D. Okumura, and T. Shibata. Grain-size dependent yield behavior under loading, unloading and reverse loading. *International Journal of Modern Physics B*, 22(31n32) :5937–5942, dec 2009.

[20] S. Forest, J. R. Mayeur, and D. L. McDowell. *Micromorphic Crystal Plasticity*, pages 643–686. Springer International Publishing, Cham, 2019.

[21] R. J. Asaro. Elastic-plastic memory and kinematic-type hardening. *Acta Metallurgica*, 23 :1255–1265, 1975.

[22] R. J. Asaro and J. R. Rice. Strain localization in ductile single crystals. *Journal of the Mechanics and Physics of Solids*, 25(5) :309–338, oct 1977.